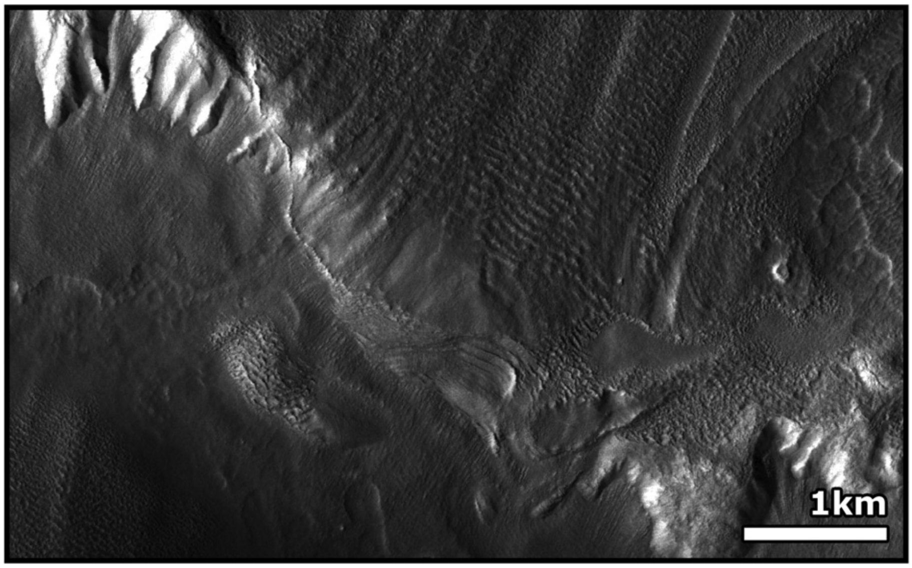

Fig. 7. CTX image of the scarp that represents the contact between the two craters (part of CTX image P01_001553_2232; context provided in Fig. 3A). Deposits from the perched crater are draped over the scarp in some places, while local areas on the eastern portion of the scarp show evidence for flow reversals towards the south.

smaller crater are draped over the scarp face with very little modification evident (Figs. 3, 4A). The minimum thickness necessary to fill the two-crater system with ice (~1000 m) is comparable to that calculated for a similar system at a similar latitude along the dichotomy boundary by Dickson et al. (2008) (~920 m). While the dichotomy boundary example occurred within a network of LVF (Dickson et al., 2008), the constrained nature of these units within a two-crater system allows for the first volumetric measurements of minimum ice necessary at this location. The very large amounts of glacial ice necessary to fill this two-crater system (at least ~750 km^3) suggest that significant accumulation occurred in this region and that Phlegra Montes, this crater in particular, and other localized traps (Safaeinili et al., 2009) hosted significant reservoirs of water ice during periods of the Amazonian when surface conditions were different from today.

4.4. Formation of concentric crater fill and localized episodic flow

Craters exhibiting CCF are common in the Phlegra Montes region (Squyres, 1979). The larger of the two craters in this study shows classic landforms consistent with those mapped using Viking data by Squyres (1979). Concentric ridges and grooves parallel to the crater rim, often lobate when viewed in detail, characterize most of the crater floor and extend ~10 km into the crater. This texture is more apparent in the southern portion of the crater, and the asymmetric (pole-facing) profile of the crater floor observed by MOLA (Fig. 2) argues for significant amounts of material transport from the southern crater rim towards the center of the crater late in the history of the deposit evolution. Given the lobate nature of these ridges, together with the supporting evidence for more extensive glaciation in this region, we propose a model of cold-based glacial flow and deposition to explain the late-stage CCF within the larger crater. We interpret the CCF texture to be representative of the waning phase of this extensive glaciation. As regional ice deposits thinned, the crater rim crests and walls became exposed, providing rocky debris to cover the glaciers. Once debris was available to create a protective layer, rates of sublimation of ice decreased, and the late-stage deposits in crater interiors were preserved (e.g., Helbert et al., 2008; Head et al., 2010-this issue). The presence of ring-mold craters (Kress and Head, 2008) in the concentric crater fill suggests that buried ice may still remain below the CCF today.

On the interior eastern rim of the larger crater (Fig. 6), we observe a ~3.25 km wide series of concentric lobes of material that are oriented towards the crater floor. These lobes are sourced from an elevated terrace along the crater wall, where CTX data show evidence for downvalley flow and constriction between obstacles, similar in nature to the “hourglass” feature on the eastern margin of the Hellas basin in the southern hemisphere (Head et al., 2005). The concentric lobes are bounded at their margins by broad ridges with convex-up profiles consistent with glacial ice. These lobes show evidence for higher concentrations of ice than the CCF nearby, and shows the variability in accumulation at various locations within the crater.

Dickson et al. (2008) found evidence for episodes of localized alpine-like valley glaciation that followed kilometer-thick-scale glaciation along the dichotomy boundary. Here we find a similar sequence of glaciation, where localized cold-trapping led to isolated flow of ice-rich material along the interior and exterior crater walls, followed by sublimation and retreat. This is most prominently displayed by the expansive units of lineated terrain (Figs. 3C, 4A). These units are characterized by downslope-trending ridges that are found atop convex-up lobes. Downslope lineations are common at the base of wet-based glacial environments on Earth (glacial scour, fluting, etc.), but these ridges occur within the unit, not at the base, and thus are not evidence for modification of the substrate. Also, the lack of evidence for wet-based glacial processes in this region (eskers, meltwater channels, etc.) lead us to consider cold-based origins to the lineated texture. We interpret these ridges to be remnants of internal flow lines or supraglacial debris, deposited within or on top of the ice-rich deposit. The valleys from which the lineated terrain are sourced reveal evidence along their walls for vertical downwasting of the ice that we interpret to have contributed to the formation of the lineated terrain. At HiRISE scale, a generally continuous ridge is observed tens of meters above the present day valley floor (Fig. 4B, C). HiRISE coverage of these features is limited to a small area at the scarp face that separates the two craters, and where the ridge is visible it can be traced along the walls of several valleys at a consistent elevation above the valley floors. This is identical to the sidewall lineations observed in a tributary valley at the dichotomy boundary by Dickson et al. (2008) in CTX data, which they interpreted to be the martian equivalent of terrestrial “trimlines,” which record the most-recent high-ice stands along the walls of glacial valleys. On Earth this is generally represented by either a contrast in albedo above and below